International Journal of Thermophysics, Vol. 26, No. 6, November 2005 (© 2005)
DOI: 10.1007/s10765-005-8587-2

Speed of Sound in Pure Water at Temperatures between 274 and 394 K and at Pressures up to 90 MPa[1]

G. Benedetto,[2] R. M. Gavioso,[2] P. A. Giuliano Albo,[2] S. Lago,[2,3] D. Madonna Ripa,[2] and R. Spagnolo[2]

A newly designed experimental apparatus has been used to measure the speed of sound u in high-purity water on nine isotherms between 274 and 394 K and at pressures up to 90 MPa. The measurement technique is based on a traditional double-reflector pulse-echo method with a single piezoceramic transducer placed at unequal distances from two stainless steel reflectors. The transit times of an acoustic pulse are measured at a high sampling rate by a digital oscilloscope. The distances between the transducer and the reflectors were obtained at ambient temperature and pressure by direct measurements with a coordinate measuring machine. The speeds of sound are subject to an overall estimated uncertainty of 0.05%. The acoustic data were combined with available values of density ρ and isobaric heat capacity c_p along one isobar at atmospheric pressure to calculate the same quantities over the whole temperature and pressure range by means of a numerical integration technique. These results were compared with those calculated from the IAPWS-95 formulation with corresponding relative deviations which are within 0.1%.

KEY WORDS: pulse-echo technique; pure water; speed of sound.

1. INTRODUCTION

Besides its basic importance in a great number of different technical and scientific applications, water is commonly used as a reference fluid for the calibration of a variety of measuring devices including experimental

[1] Paper presented at the Fifteenth Symposium on Thermophysical Properties, June 22–27, 2003, Boulder, Colorado, U.S.A.

[2] Istituto Elettrotecnico Nazionale Galileo Ferraris, Strada delle Cacce 91, I-10135 Torino, Italy.

[3] To whom correspondence should be addressed. E-mail: lago@ien.it

apparatus for the measurement of the speed of sound in liquids. As a part of an ongoing research program to develop an accurate experimental technique for the measurement of speed of sound in high pressure liquids, we considered the possibility of avoiding such a calibration procedure, and obtain at the same time values of speed of sound in pure water of high accuracy. The speed of sound in water as a function of temperature and pressure has been extensively measured by the application of a variety of methods; nevertheless, results of very high accuracy are typically available only at atmospheric pressure [1, 2], or over a limited range of temperature at higher pressures [3–5].

In this work we report measurements of the speed of sound u in pure water at temperatures between 274 and 394 K and at pressures up to 90 MPa. These results have been compared to those calculated from the IAPWS-95 formulation [6] and are in agreement within 0.1% over the complete temperature and pressure range investigated here.

Accurate measurements of the speed of sound in real fluids have special interest as they offer an indirect way to obtain information on related thermodynamic properties like density and heat capacity, whose direct measurement, especially at high pressure, is extremely difficult. In order to test this possibility, we combined our acoustic data with values of density ρ and isobaric specific heat capacity c_p calculated from Ref. 6 on one isobar at 0.1 MPa and, by means of the integration technique described below, determined the same quantities over the entire P–T region investigated in this study.

2. EXPERIMENTAL

The design of the present ultrasonic apparatus is based on the double reflector pulse-echo technique [7, 8] and has been chosen because of its good combination of design simplicity and high achievable resolution and accuracy.

2.1. Ultrasonic Cell

A diagram of the ultrasonic cell is shown in Fig. 1. It is made of a hollow AISI 303 stainless steel cylinder (77 mm long, 43 mm o.d., 33 mm i.d.) in which the ultrasonic transducer, a piezoelectric ($PbZrTiO_3$ – Channel Industries mod. C5400) disk (10 mm diam., 0.5 mm thickness), is clamped at its edges between a conical support and a conical Teflon insulated stainless steel ring. The conical shape of the ring and the support minimizes the interfering effect of diverging components of the acoustic beam which may be reflected on the transducer. The ring and the support

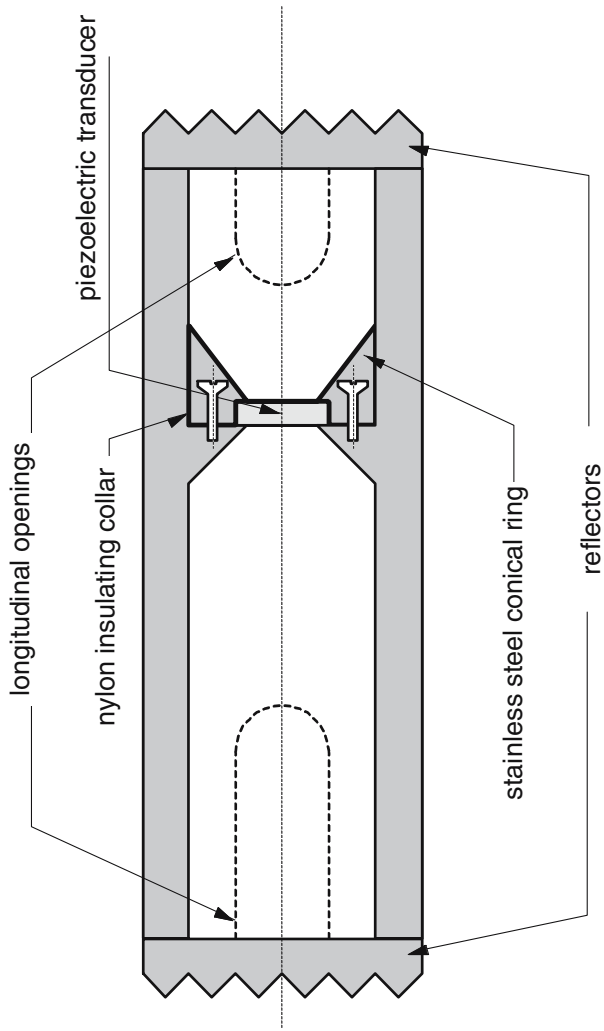

Fig. 1. Ultrasonic cell for measurement of speed of sound in high-pressure liquids.

are fixed to each other by means of three screws electrically insulated by small Teflon collars. Two solid stainless steel reflectors (15 mm thickness) having plane smooth surfaces are fixed to the ends of the cell at distances of 30.5 and 46 mm from the source. The outer surfaces of the reflectors were cut with a series of pyramid-shaped incisions in order to

maximize dispersion of sound passing through the reflectors, thus avoiding back-reflection into the cell.

2.2. Measurement of Propagation Time

Ultrasonic measurement of the speed of sound consists basically of the determination of two mechanical quantities: a geometric acoustic path and the associated time interval. According to the double reflector pulse-echo technique, a function generator (Agilent 33250A) excites a piezo-ceramic transducer with an electrical signal in the form of ten-cycle repeated tone bursts with a carrier frequency of about 5 MHz and an amplitude of $10\,V_{p-p}$. The transducer emits two acoustic pulses spreading simultaneously in opposite directions. Each acoustic wave train, hitting the reflector, produces a set of echoes. The electrical signal delivered to the transducer and the echoes from the reflectors are recorded by a digital oscilloscope (LeCroy LT372). The burst period is chosen low enough to obtain the complete decay of the echoes before the triggering of the next electrical pulse. The complete waveform corresponds to a duration of $100\,\mu s$ and is digitized at a sampling rate of 4×10^9 samples per second. The digital signal $P_1(t_i)$, representing the first sampled echo coming from the nearest reflector, is correlated to the first echo $P_2(t_j)$ from the farthest reflector by means of a temporal correlation function $C(\tau)$,

$$C(\tau) = \int_{-\infty}^{+\infty} P_1(t) P_2(t+\tau)\, dt, \tag{1}$$

where $\tau \in]-\infty, +\infty[$ is a point in the delay-time domain. A fast and reliable method to accomplish this calculation is based on the FFT algorithm and the properties of Fourier transforms: applying the Fourier operator $F[\cdots]$ to both sides of Eq. (1), we get

$$F[C] = F[P_1]^* \, F[P_2]. \tag{2}$$

The correlation function is obtained at the cost of two FFT transforms and a final inverse transform on $F[C]$. The delay time between the two echo waveforms $P_1(t_i)$ and $P_2(t_j)$ is assumed to be the value $\tau_{\exp}$ that maximizes the function $C(\tau)$. This method has the advantage of being insensitive to amplitude differences between the two echo waveforms. The performance of the algorithm has been tested against synthetic data and found to be very robust; the addition of Gaussian noise with an amplitude equal to 10% of the maximum signal produced a difference of only one sampling interval in the determination of the delay time.

Since the sound speed of interest is associated with the idealized condition of perfect plane waves traveling in free-space, the measured transit time difference $\tau_{\exp}$ has to be corrected for diffraction effects. Diffraction causes the wave fronts produced by a finite dimension source to lay on curved surfaces and consequently generates a phase shift $\phi(L)$ relative to a plane wave traveling the same distance. The measured transit time difference $\tau_{\exp}$ must then be increased by $\delta\tau$;

$$\delta\tau = \frac{\phi(2L_2) - \phi(2L_1)}{\omega_0}, \tag{3}$$

$$\phi(L) = Arg\left(1 - \frac{4}{\pi}\int_0^{\pi/2} \exp\left[-i\left(\frac{2\omega_0 b^2}{uL}\right)\cos^2\vartheta\right]\sin^2\vartheta\, d\vartheta\right), \tag{4}$$

where ω_0 is the angular frequency of the carrier, u is the sound speed, L_1 and L_2 are the distances between the source and the reflectors, and b is the source radius. The measured speed of sound is obtained as $u_{\text{meas}} = \frac{2\Delta L(T,P)}{\tau_{\text{corr}}}$, where $\Delta L = L_2 - L_1$ and $\tau_{\text{corr}} = \tau_{\exp} + \delta\tau$. Considering the mutual dependence of $\delta\tau$ and u_{meas}, their values are found by iteration. The diffraction correction for our experimental apparatus amounted to less than 0.015% of the measured transit time difference.

2.3. Dimensional Measurements

A coordinate measuring machine was used to determine the difference ΔL between the lengths of the acoustic paths L_1 and L_2. The machine had a resolution and a repeatability of $0.1\,\mu$m and an uncertainty of approximately $1\,\mu$m. Measurements were carried out in a thermostatted room at ambient temperature T_0 and pressure P_0. Five successive measuring sequences were accomplished, each one consisting of nine randomly spaced points on the two surfaces of the PZT transducer and the flat faces of the cell sidewall. The maximum difference between the five evaluations of $L_{1,2}$ was less than $1\,\mu$m. Although it is likely that the major unknown systematic uncertainty components associated with the coordinates measurement would cancel out in the difference operation, we estimated uncertainty of $\pm 2\,\mu$m for the measured values $L_1 = 30.592$ mm and $L_2 = 45.997$ mm. Finally, the difference in the acoustic path was $\Delta L = 15.405 \pm 0.004$ mm.

The variation of ΔL with temperature and pressure was calculated as $\Delta L(T, P) = \Delta L(T_0,\ P_0)(1 + \alpha\Delta T - \beta/3\Delta P)$ where α and β are, respectively, the linear coefficient of thermal expansion and the adiabatic coefficient of the compressibility of stainless steel [9]; the latter was

calculated from the values of the elastic constants of the same material. The magnitude of the corrections required for the path length was 0.48% at the maximum pressure (90 MPa) and temperature (394 K).

2.4. High-Pressure System

The high-pressure system consists of three main sections: the pressure vessel, a pressure monitoring and measuring line, and a pressure control device. The vessel and the measuring line can be completely isolated from the other parts of the system in order to minimize heat exchange effects between the thermostatted vessel and the ambient environment. Pressure is generated and controlled by a 100 MPa pressure amplifier connected to an ambient pressure liquid reservoir which contains the sample under test. A pressure transducer (Sensotec TJE/4843–01) was used to measure the pressure in the system with an uncertainty of 0.04 MPa as estimated from the calibration between 20 and 90 MPa against a pressure balance (national standard). The pressure vessel, specifically designed for this application, is made from a stainless steel alloy and has an internal volume of 420 cm^3. It is provided with two coaxial pressure-tight electrical feedthroughs for high frequency signals transmission to the ultrasonic cell and can be operated at pressures up to 100 MPa and in a temperature range of 230–400 K.

2.5. Temperature Measurement and Control

The ultrasonic cell and the pressure vessel were placed in a stirred liquid bath thermostat based on a Dewar vessel with a capacity of approximately 60 dm^3. Heat losses through the wall and the lid of the vessel were further reduced with a 7 cm thick polystyrene insulating coating. The fluid within the bath was a silicone oil (Dow Corning 200/100 cs). The temperature was maintained and controlled by a system consisting of a main thermostat (Julabo FP50) having a stability of ± 0.01 mK, and a proportional-integral-derivative controller operating with a platinum resistance probe and a 60 W incandescence bulb which served for the control heater. This system was used to achieve a long-term temperature stability within the bath of ± 2 mK over the whole operating temperature range. The temperature associated with speed-of-sound measurements was determined with an uncertainty of ± 0.01 K as the average of the readings of two platinum resistance thermometers (PRTs), calibrated by comparison with a standard PRT, which were attached to the top and bottom parts of the pressure vessel. The temperature gradient recorded by the two PRTs in the course of the present speed-of-sound measurements was within 10 mK, with the exception of the lowest isotherm at 274 K; in this case, the top of

the vessel was 20 mK warmer than the bottom suggesting that a thermal link from the top to ambient temperature existed.

2.6. Purity of Water Sample

The deionized water sample used in this study had a specified minimum purity of 99.99% by volume. It has been obtained by means of an active resins filtering device (Millipore) with a stated electrolytic conductivity of $0.054\,\mu S \cdot cm^{-1}$ and a concentration of particles ($0.22\,\mu m$) < 1/ml; however, it is likely that this extremely high level of deionization and purity of the water sample was substantially reduced as the sample came in contact with the different metal parts composing the experimental apparatus. The ultrasonic cell was filled under vacuum.

3. RESULTS

3.1. Speed of Sound in Water: Results and Comparison with IAPWS-95

The experimental values of the speed of sound u in water at 90 points are listed in Table I and represented in Fig. 2 as a function of temperature and pressure. These measurements were carried out on nine isotherms between 274 and 394 K, in approximately 10 MPa pressure decrements from 90 MPa to atmospheric pressure, with the exception of the isotherms at 379 and 394 K where low pressure readings were limited to a minimum of 10 MPa, due to the sample being in the vapor state at atmospheric pressure. Since an adiabatic decrease in pressure of 10 MPa changed the temperature inside the pressure vessel and the ultrasonic cell, it was necessary to wait approximately 1 h until, according to the indications of the two thermometers attached to the pressure vessel, thermal equilibrium was reestablished and a new measurement was made. Figure 2c shows intersecting isotherms; this is to be expected since u decreases at low pressure for temperatures higher than ~ 347.2 K [10]. The characteristic shift of the speed-of-sound maximum towards higher temperatures as a function of increasing pressure can be observed in Fig. 2d.

We have compared our results to the predictions of the formulation of the International Association for the Properties of Water and Steam (IAPWS-95) [6]. The estimated uncertainty of the formulation in speed of sound ranges from $\pm 0.005\%$ at atmospheric pressure to a maximum of $\pm 0.1\%$ over the P–T region of interest for our measurements. As represented in Fig. 3, most of our results show deviations from IAPWS-95 which are within 0.05%, with the exception of the lowest and highest temperature isotherms at 274 and 394 K where deviations are within 0.1%.

Table I. Experimental Values of Speed of Sound in Water

p (MPa)	u ($m \cdot s^{-1}$)	p (MPa)	u ($m \cdot s^{-1}$)	p (MPa)	u ($m \cdot s^{-1}$)	p (MPa)	u ($m \cdot s^{-1}$)	p (MPa)	u ($m \cdot s^{-1}$)
T = 273.98 K									
0.09	1406.04	20.00	1437.35	40.03	1471.26	60.05	1506.71	79.96	1543.00
10.00	1421.25	30.01	1454.05	50.04	1488.84	70.09	1524.95	89.94	1561.31
T = 289.01 K									
0.09	1468.43	20.02	1500.96	40.02	1534.46	59.97	1568.35	80.03	1602.59
0.17	1468.57	30.04	1517.68	50.05	1551.44	70.04	1585.53	90.00	1619.64
10.04	1484.56								
T = 303.99 K									
0.10	1510.61	20.05	1544.26	39.98	1577.80	60.06	1611.42	80.11	1644.77
0.18	1510.76	30.05	1561.11	50.06	1594.71	70.00	1627.98	90.01	1661.14
10.02	1527.37								
T = 319.00 K									
0.09	1537.16	20.10	1572.22	40.09	1606.52	59.99	1640.14	80.10	1673.45
10.07	1554.73	29.95	1589.20	50.07	1623.46	70.01	1656.84	90.00	1689.64
T = 334.00 K									
0.09	1551.17	19.90	1587.38	40.07	1623.16	60.02	1657.59	79.99	1691.11
10.00	1569.43	30.13	1605.65	50.11	1640.66	70.10	1674.60	90.00	1707.59
T = 349.00 K									
0.09	1554.92	20.00	1593.14	39.89	1629.85	60.00	1665.68	79.99	1700.01
10.17	1574.45	30.00	1611.76	50.12	1648.22	70.07	1683.08	90.02	1716.83
T = 364.00 K									
0.09	1549.99	20.02	1590.45	40.04	1629.15	60.15	1666.36	79.99	1701.58
9.99	1570.35	30.01	1609.99	49.77	1647.37	70.06	1684.09	90.09	1719.00
T = 379.00 K									
10.05	1559.21	30.01	1600.94	50.00	1640.57	70.12	1678.50	90.06	1714.66
20.06	1580.44	40.06	1621.12	59.97	1659.60	79.88	1696.31		
T = 394.00 K									
10.16	1542.62	30.01	1586.75	49.98	1628.50	69.89	1667.71	90.02	1705.48
20.15	1565.19	39.96	1607.85	59.97	1648.41	80.10	1687.10		

The smoothness and low scatter of the deviations, as evident on the scale of Fig. 3, show the satisfactory level of precision achieved with the present experimental apparatus and measurement procedures.

3.2. Estimation of the Measurement Uncertainty

From a metrological point of view, the pulse-echo technique for sound-speed determination is an indirect measurement method described by the following model:

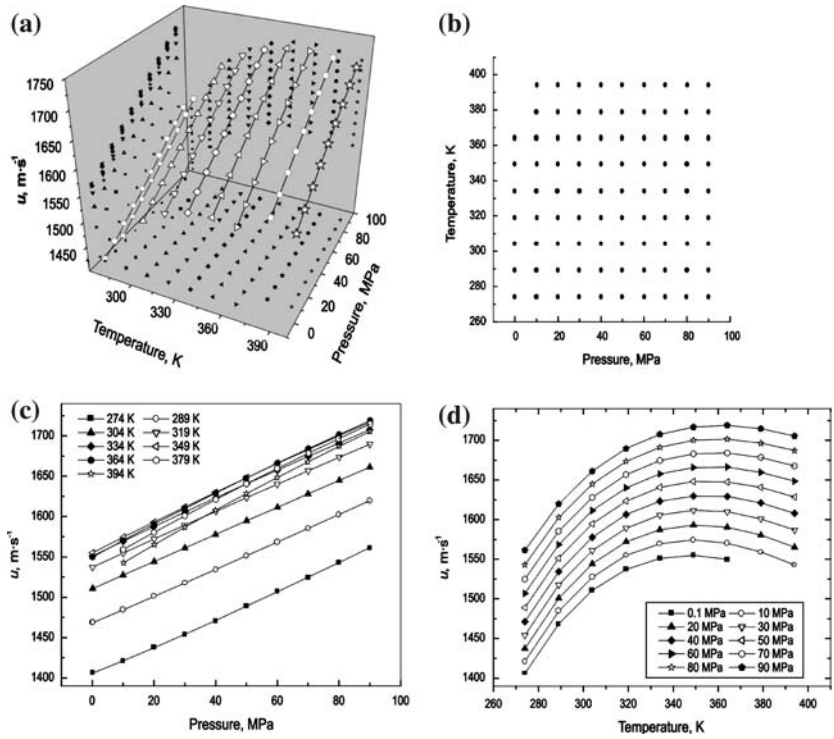

Fig. 2. Speed of sound of water: (a) as function of pressure and temperature; (b) investigated P–T region; (c) isotherms as a function of pressure; and (d) isobars as a function of temperature.

$$u_{\text{meas}} = u\,(\Delta L, \tau, T, P) = \frac{2\Delta L}{\tau}, \tag{5}$$

where ΔL and τ are independent mechanical determinations and P, T are state variables. Consequently, standard equations for error propagation can be applied, expressed as

$$\frac{\sigma\,(u_{\text{meas}})}{u_{\text{meas}}} = \sqrt{\left(\frac{\sigma\,(\Delta L)}{\Delta L}\right)^2 + \left(\frac{\sigma\,(\tau)}{\tau}\right)^2 + \left(\frac{T}{u_{\text{meas}}}\frac{\partial u}{\partial T}\right)^2 \left(\frac{\sigma\,(T)}{T}\right)^2 + \left(\frac{P}{u_{\text{meas}}}\frac{\partial u}{\partial P}\right)^2 \left(\frac{\sigma\,(P)}{P}\right)^2}. \tag{6}$$

Table II lists the major components of the standard uncertainty from the measurement of the quantities in Eq. (6). Evaluating the uncertainty

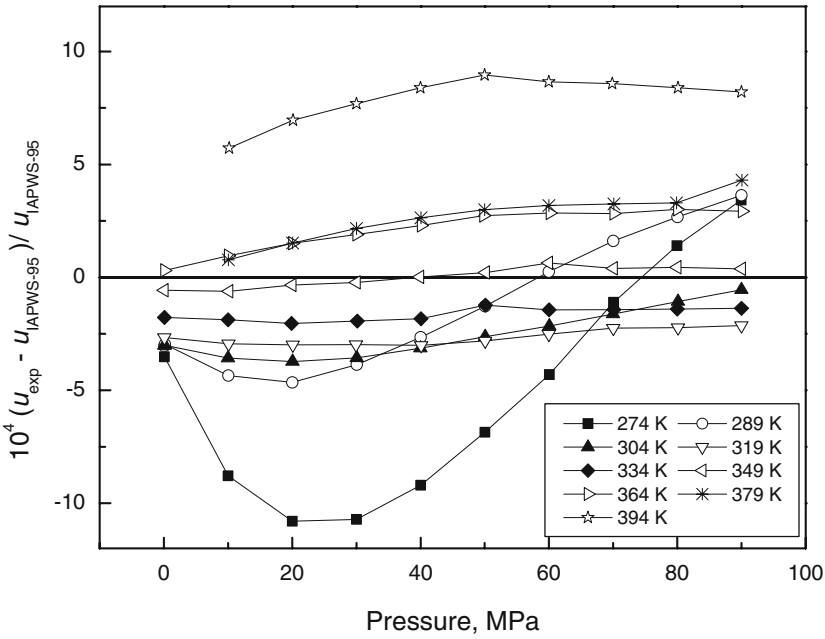

Fig. 3. Deviations of experimental speed of sound of water from IAPWS-95 formulation.

related to the determination of the acoustic path lengths, we do not take into account the contribution of α and β parameters which appear in the correction formula discussed in Section 2.3. The uncertainty associated with time-delay measurements is assumed to be equal to 0.5 ns, corresponding to two oscilloscope sampling intervals; however, the high signal-to-noise ratio in the resulting waveforms and the very good resolution of the pulse correlation technique could further reduce this value. Temperature measurements are assumed to be affected by an uncertainty

Table II. Uncertainty Budget

Uncertainty Source		Relative Magnitude
Determination of the acoustic path	$\sigma(\Delta L)/\Delta L$	0.026%
Determination of temporal delay	$\sigma(\tau)/\tau$	0.002%
Temperature measurements	$\left(\frac{\partial u}{\partial T}\right)\frac{\sigma(T)}{u}$	0.003%
Pressure measurements	$\left(\frac{\partial u}{\partial P}\right)\frac{\sigma(P)}{u}$	0.030%
Estimated Overall Uncertainty		$< 0.050\%$

of 0.01 K, corresponding to the calibration accuracy. The need to correct from the experimental to the reported values of the intrinsic parameters P and T introduces an equivalent uncertainty in the sound speed. Also, the uncertainty in the determination of the thermodynamic speed of sound depends on the uncertainty in the association of the measured speed-of-sound values with the effective thermodynamic P–T state of the sample. In this framework, our pressure measurement plays a major role in the magnitude of the overall uncertainty, due to the relatively large uncertainty (± 0.04 MPa) of the pressure transducer in the low pressure region (0.1 to 10 MPa). The estimated relative uncertainty, considered to be representative over the entire pressure range, has been calculated by a weighted mean; the sensibility factors $\left(\frac{T}{u_{\text{meas}}}\frac{\partial u}{\partial T}\right)$ and $\left(\frac{P}{u_{\text{meas}}}\frac{\partial u}{\partial P}\right)$ which appear in Eq. (6) have been derived from the experimental sound speeds by means of a polynomial interpolating function. Finally, the relative uncertainty in sound speed values is estimated to be 0.05% over the entire P–T region examined.

3.3. Derivation of Density and Isobaric Specific Heat Capacity

From the experimentally determined sound-speed data points, it is possible to work out the density function $\rho(T, P)$, i.e., the equation of state of the fluid under test, and the isobaric specific heat capacity function $c_p(T, P)$ over the P–T region examined, given a set of independent ρ and c_p determinations on a single (but otherwise arbitrary) isobar. The starting relations are

$$\left(\frac{\partial \rho}{\partial P}\right)_T = \frac{T\alpha_P^2}{c_P} + \frac{1}{u^2}, \tag{7}$$

$$\left(\frac{\partial c_P}{\partial P}\right)_T = -\frac{T}{\rho}\left[\alpha_P^2 + \left(\frac{\partial \alpha_P}{\partial T}\right)_P\right], \tag{8}$$

$$\alpha_P = -\frac{1}{\rho}\left(\frac{\partial \rho}{\partial T}\right)_P, \tag{9}$$

where α_P is the thermal expansion coefficient and u is the sound speed. Given a suitable initial condition, in the form of $\rho(T, P_0)$ and $c_P(T, P_0)$ functions at the starting pressure P_0, Eqs. (7)–(9) form a complete first-order differential equation set that can be integrated over the entire pressure range covered by the $u(T, P)$ function.

We used a Cash-Karp, adaptive step-size Runge–Kutta method which provides a fifth-order approximation to differential systems. Sound-speed experimental data have been interpolated by means of the Akima algorithm [11], a locally bivariate quintic polynomial generator, in order to produce an orthogonal mesh of sound-speed values in the P–T space. The set of Eqs. (7)–(9) was then integrated over the entire pressure and temperature range, using a B-SPLINE sixth-order interpolating function to calculate the derivatives which appear in Eqs. (7)–(9). The integration program proceeded along nine isothermal lines starting from atmospheric pressure, apart from the last two isotherms (379 and 394 K), which started from 10.0 MPa.

The integration procedure was first tested on speed-of-sound data drawn from Ref. 6 and found to reproduce density values from the same source with a maximum relative deviation of 1 ppm. The corresponding agreement for isobaric heat capacities was within 2×10^{-4} with the only exception for the lower isotherm at 274 K, whose maximum deviation from reference values was 2×10^{-3}. We consider this problem to be the result of the inaccurate evaluation of derivatives that appear in the right side of Eq. (8) for points on the boundary of the integration region, as pointed out in Ref. 5.

A comparison between density data, calculated with the procedure discussed above from our experimental values of sound speed and the reference values from IAPWS-95, is shown in Fig. 4a; it can be noted an overall good agreement, apart from the above mentioned anomaly at 274 K (the reported relative uncertainty for IAPWS-95 density data is $\pm 10^{-5}$). In Fig. 4b, the results of an analogous comparison for the calculated isobaric heat capacities is shown; the anomalous 274 K isotherm has been eliminated to enhance graphical presentation. Apparently the greater deviations for the isotherm at 394 K are determined by the corresponding greater sound-speed deviations from reference values which directly influence the algorithmic reconstruction of the $c_p(T, P)$ function.

4. CONCLUSIONS

Speed-of-sound measurements on samples of purified water in an extended region of P–T space have been used to test a newly assembled ultrasonic apparatus against available literature data. The results and the uncertainty evaluation demonstrate good performance of the whole measurement system and suggest further improvements: a better precision and accuracy in the thermodynamic point determination (the uncertainty budget reported in Table II indicates the role of pressure sensors as precision-limiting devices) and an improved piezo-clamping mechanism to guarantee

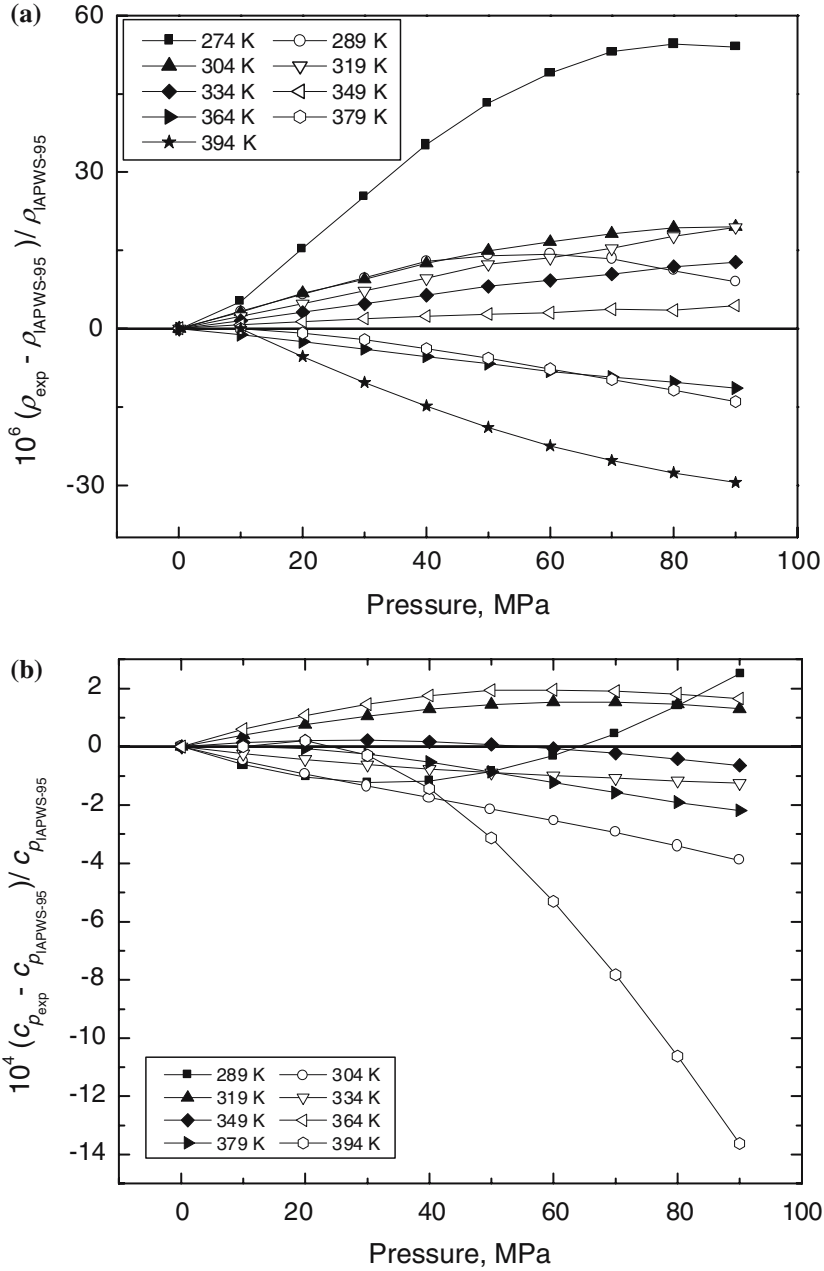

Fig. 4. (a) Deviations of calculated densities of water from IAPWS-95 formulation and (b) deviations of calculated isobaric heat capacities of water from IAPWS-95 formulation.

a higher degree of parallelism between the ultrasonic source and the reflectors, reducing the uncertainty in the evaluation of the acoustic paths.

REFERENCES

1. V. A. Del Grosso and C. W. Mader, *J. Acoust. Soc. Am*. **52**:1442 (1972).
2. K. Fujii and R. Masui, *J. Acoust. Soc. Am*. **93**:276 (1993).
3. K. Fujii, Paper presented at the 12th Symp. Thermophys. Props., Boulder, Colorado (1994).
4. A. A. Alexandrov and A. I. Kochetov, *Therm. Eng*. **26**:558 (1979).
5. J. P. Petitet, R. Tufeu, and B. Le Neindre, *Int. J. Thermophys*. **4**:35 (1983).
6. W. Wagner and A. Pruss, *J. Phys. Chem. Ref. Data* **31**:387 (2002).
7. P. J. Kortbeek, M. J. P. Muringer, N. J. Trappeniers, and S. N. Biswas, *Rev. Sci. Instrum*. **56**:1269 (1985).
8. S. J. Ball and J. P. M. Trusler, *Int. J. Thermophys*. **22**:427 (2001).
9. ASM International Handbook Commiteee, J. R. Davis, ed., in *ASM Specialty Handbook–Stainless Steels*, (ASM International, Materials Park, Ohio, 1994).
10. W. D. Wilson, *J. Acoust. Soc. Am*. **31**:1067 (1959).
11. H. Akima, *ACM Trans. Math. Software* **4**:148 (1978).